The Leidenfrost transition of water droplets impinging onto a superheated surface

Guillaume Castanet, Ophélie Caballina, W. Chaze, R. Collignon, F. Lemoine

The Leidenfrost transition of water droplets impinging onto a superheated surface

G. Castanet*, O. Caballina, W. Chaze, R. Collignon, F. Lemoine

Université de Lorraine, CNRS, LEMTA, F-54000 Nancy, France

Keywords:
Drop impact
Leidenfrost temperature
Transition boiling
Film boiling
Laser-induced fluorescence
Infrared thermography

A B S T R A C T

Water droplets impinge on a sapphire wall heated to a temperature ranging from 300°C to 700°C. Advanced measurement techniques are used to characterize the thermal processes associated with the drop impact. IR thermography, implemented by coating the impacted surface with an opaque and emissive material in the IR domain, makes it possible to measure the temperature of the solid surface during the impact process. Laser-induced fluorescence imaging is used to characterize the temperature field in the spreading droplet. At the onset of film boiling, the temperature distribution on the solid surface is marked by the formation of a fingering pattern. This latter corresponds to spatial fluctuations in the thickness of the vapor film. When a water droplet hits an overheated wall with a significant impact velocity, the thermal contact is so rapid and intense that the liquid temperature can largely overtake the saturation temperature and reach the spinodal temperature, i.e. the highest temperature at which water can exist in the liquid state. In this situation, experiments show that the dynamic Leidenfrost point is directly linked to the spinodal temperature. A superheating of the liquid by several hundred of °C and the subsequent homogeneous nucleation, have to be considered to describe the heat transfer in the film boiling regime.

1. Introduction

The impact of liquid droplets on overheated solid surfaces is a phenomenon that is found in many industrial applications, such as the quenching of metal surfaces in the steel industry, loss-of-coolant accident (LOCA) in nuclear facilities, direct injection in diesel and gasoline engines where fuel droplets collide with the overheated surface of the piston. In many technological processes, spray cooling is used when it is required to obtain a rapid and efficient cooling of hot surfaces. However, one of the main challenges is to control the heat flux from the solid surface through the boiling process. Numerous studies have been motivated to obtain quantitative information, but it is still difficult to obtain the physical understanding of the boiling process during the drop impact. Quantitative measurements have been constrained by several difficulties, including the very fast dynamics of the drop and bubble formation, the lack of optical access for observing under the droplet close to the solid surface. So far, most attention has been focused on determining the different boiling regimes and the transition between them, but relatively little is still known about the dependence of the heat flux on the physical parameters.

When the temperature of the solid surface is higher than the saturation temperature of the liquid, the phase change due to the intense heat transfer radically modifies the droplet impact dynamics compared to an isothermal impact [1,2]. Maps of impact regimes have been established for various surface temperatures and impact conditions by authors like Bernardin et al. [3], Tran et al. [4] and Bertola [5]. A fairly comprehensive review of the phenomena associated with the interaction between a droplet and a very hot surface can be found in review papers such as Liang and Mudawar [6]. Because of the different phenomena associated with the boiling (namely drop evaporation, Marangoni related effects, nucleate boiling, transition boiling, film boiling), the heat flux is not a monotonous function of the surface temperature. It is widely considered that its minimum value occurs at the so-called Leidenfrost point (LFP) which separates two major boiling regimes: the transition boiling regime and the film boiling regime. In the boiling film, the droplet sits on a vapor cushion that prevents a direct contact with the solid surface. The very low thermal conductivity of the vapor means that heat transfer is quite low in this regime. In the transition boiling regime, liquid contact occurs with portions of the surface, resulting in a significant improvement in heat transfer compared to film boiling.

To predict the LFP, several models and correlations have been proposed [7,8]. These are based in several hypotheses including a Taylor-like hydrodynamic instability that can disrupt vapor pock-

* Corresponding author.
E-mail address: guillaume.castanet@univ-lorraine.fr (G. Castanet).

Nomenclature

f	Acquisition frame or repetition rate [Hz]
t	Time [s]
T	Temperature [°C]
T_{cw}	Critical temperature associated with the wetting of the solid surface [°C]
d	Droplet diameter [m]
We	Weber number defined by $We = \rho_l U d/\gamma$
U	Drop impact velocity [m/s]
m	Mass of the droplet [kg]
q	Heat flux density [W/m^2]
L_v	Latent heat of vaporisation [J/kg]
Q	Heat [J]
Q_{vap}	Heat used for droplet vaporization [J]
e	Thermal effusivity [W.K^{-1}.m^{-2}.s$^{1/2}$]
Cp	Heat capacity [J/(kg.K)]
R_s	Droplet spreading radius [m]
R_w	Radius of the wetted area [m]
r	Radial distance to the drop center [m]
N	Number of fingers
u	Velocity in the liquid phase [m/s]
LFP	Leidenfrost point [°C]
h_l	Lamella thickness [m]
h_t	Thickness of the thermal boundary layer [m]
E	Liquid disk thickness [m]

Greek symbols

μ	Dynamic viscosity [Pa.s]
γ	Surface tension [N.m^{-1}]
κ	Thermal conductivity [W.m^{-1}.K^{-1}]
ρ	Density [kg/m^3]
λ	Wavelength [m]
ε	Spectral emissivity
θ	Azimuth angle [°]
ξ	Self-similar variable

Subscripts

S	At the wall surface
l	The liquid phase
v	The vapor phase
w	The solid wall
d	Droplet
sat	Saturation condition
0	Initial condition (before the drop impact)
$spin$	Spinodal limit
c	Thermal contact
lv	At liquid-vapor interface

ets, or an explosive boiling caused by homogeneous nucleation. The maximum attainable temperature to which a liquid can be heated before it vaporizes spontaneously, can be determined theoretically based on thermomechanical stability from the equation of state such as Van der Waals (the spinodal limit in the domain of metastable states is T_{spin}=320.25°C for pure water at one bar, as calculated with the Wagner and Pruß equation of state [9]) or from the kinetic homogeneous nucleation theory (molecular fluctuations occur in such a way to cause a localized decrease in the liquid density, leading to the formation of vapor embryos) [7,10]. Therefore, a physical contact between the liquid phase and the solid surface is only possible if the cooling is strong enough to have the surface temperature lower than this limit. However to many authors [7,11], it is doubtful that a model for homogeneous nucleation could explain all the experimental observations for the Leidenfrost transition. For instance, experiments have shown a dependence of the LFP on the surface properties [7,12,13] and an increase of the LFP with the impact velocity [4]. But many of the LFP investigations performed so far were rather qualitative or limited to sessile droplets.

Recently, Khavari et al. [14] developed an optical method based on total internal reflection (TIR). The latter allows revealing the formation of a fingering pattern in the boiling transition regime when applied to impinging ethanol droplets (Fig. 1). The fingers can be easily distinguished from white spots and pockets observed at lower surface temperature in the bubbly boiling regime. The regularity of these fingers is striking and may suggest that a type of instability controls the number and position of the fingers. The nature of the instability (Rayleigh-Taylor or Rayleigh-Plateau) is not the focus of this study. In fact, both can be relevant to some extent [31]. Khavari et al. [14] also pointed out that the Leidenfrost transition is not an abrupt change between the 'contact-boiling' regime characterized by a violent bubbling, and the film boiling regime where the droplet never physically touches the solid surface. Their results indicate that the wetting area decreases continuously as the wall temperature approaches the LFP. Since heat transfer is mostly through the wetting surface area, a reduction of the wetting contact area seems congruent with the general idea of a heat transfer reduction when approaching the LFP. However, direct measurements of the heat transfer would supplement these observations as they will provide quantitative information on the surface temperature and local heat flux, which are key parameters to describe the boiling. These measurements are also likely to provide data on the cooling efficiency which could be valuable for cooling applications. Chaze et al. [15] demonstrated that it is possible to use IR thermography to reconstruct the time and space distribution of the wall heat flux during the impact of a droplet onto an superheated surface. Using this technique, Castanet et al. [16] could determine the evolution of the vapor film thickness in the film boiling regime for the case of ethanol droplets. In another study, Chaze et al. [17] made use of the so-called two-color laser-induced fluorescence (2cLIF) thermometry to characterize the temperature of water droplets in the film boiling regime. In the present study, the above-mentioned measurement techniques (IR thermography and 2cLIF) is used to characterize the heat transfer in the Leidenfrost transition for an impinging water droplet.

2. Experimental set-up and measurement techniques

A syringe is used to produce water drops with a diameter d of 2.6 mm (Fig. 2). After detachment from the needle of the syringe, the falling water droplets impinges on a sapphire window (25.4 mm in diameter and 5 mm thick) placed on a steel holder which is heated by cartridge heaters. In the present study, the initial temperature of the sapphire is changed between 300°C and 700°C. The impact velocity of the droplet is adjusted by changing the needle's height. In the following, the Weber number $We = \rho_l U_0^2 d/\gamma$ ranges between 17 and 140. Owing to the high thermal conductivity of sapphire κ_w, the temperature of the solid surface T_S is uniform and almost equal to the temperature of the steel holder before the drop impact. A water-cooled protective plate is required to prevent the liquid from heating up inside the needle used to produce the droplet.

Temperature measurement and heat flux reconstruction at the solid surface using IR thermography The temperature of the impact surface is characterized by means of an IR camera (FLIR ORION SC7000), which incorporates a cooled InSb detector operating in the 1.5 to 5.5 µm infrared waveband. The IR camera is equipped with a high magnification objective allowing a field of view of about 7 mm. The beginning of the acquisition by the camera is triggered by the passage of the droplet across an optical barrier (Fig. 2). The latter consists of a laser diode and a photodiode,

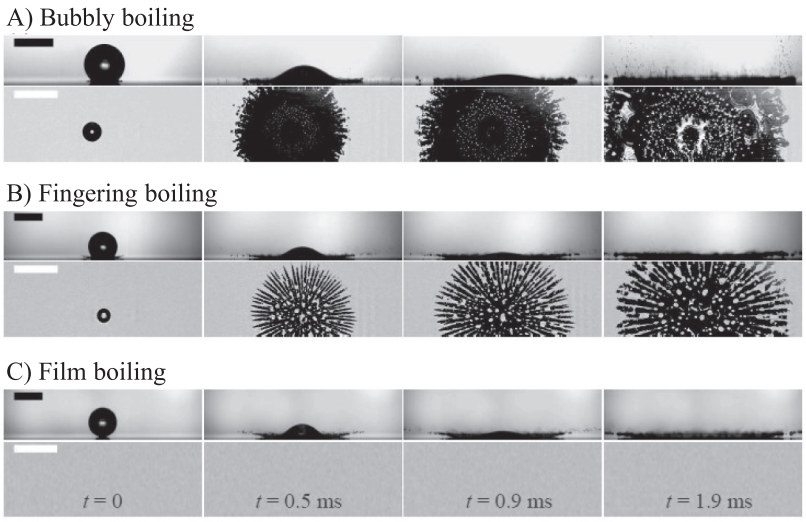

Fig. 1. Three boiling regimes identified by Khavari et al. [14] in the case of an ethanol drop impinging on a NB7 glass substrate (We=481). These regimes correspond to different wall temperatures: T_{w0}=180°C for bubbly boiling (A), T_{w0}=200°C for fingering boiling (B), T_{w0}=300°C for film boiling (C). For the latter, the thickness of the vapor film is large enough so that no evanescent waves can be transmitted to the liquid/vapor interface. This typically occurs for a thickness larger than a few hundreds of nm. All the inset bars indicate a length scale of 2 mm. Reproduced from Ref.[14]. with permission from The Royal Society of Chemistry.

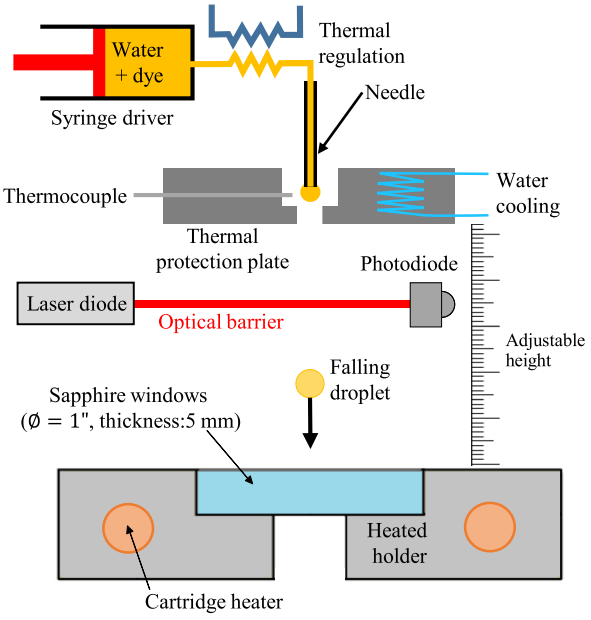

Fig. 2. The experimental setup.

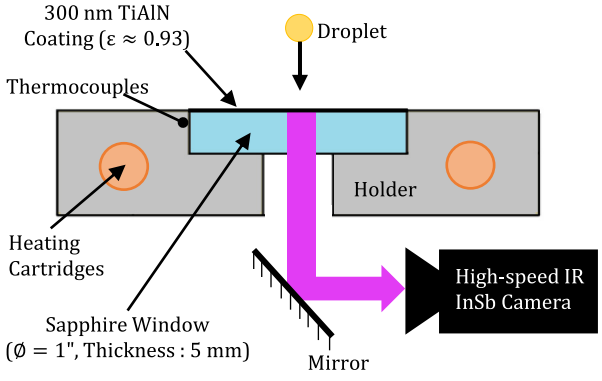

Fig. 3. Optical setup used for the visualization of the temperature field at the impact surface by IR thermography.

which are placed opposite each other. When a droplet crosses the light beam of the laser diode, a variation in light transmission to the photodiode can be detected. The system has an electron jitter of 10 µs, which is very low compared to the duration of the impact process (several ms). Bottom view images of the impacted surface are recorded thanks to the transparency of the sapphire substrate in the IR domain below 5 µm (Fig. 3). The top face of the sapphire window, where the impacts take place, is coated with a nanolayer of TiAlN (300 nm in thickness) which is resistant to high temperature. TiAlN has a high emissivity in the detection band of the camera ($\varepsilon \approx 0.93$). A benefit of this high emissivity is that the radiative emission from the surface is sufficiently large to have integration times of a few tens of µs and a very limited contributions of ambient radiations (especially those coming from the heated holder). The small thickness of the TiAlN coating allows considering that the temperature measured by IR is the temperature at the upper surface of the sapphire T_S.

The distribution of the local heat flux at the wall surface q_w can be reconstructed from the IR images using the method proposed by Chaze et al. [15]. Considering an axisymmetric heat conduction problem in the sapphire, the transient heat transfer equation in the cylindrical coordinates can be rewritten using transformations of Hankel in space and Laplace in time. An inverse heat conduction problem can be solved using the so-called quadrupole method [18] in order to obtain an analytical relationship between the measured temperature T_S and the heat flux q_w at the upper surface of the solid wall, where the drop impact is taking place. In practice, a windowing of the image is necessary to increase the frame rate of the IR camera and accurately reconstruct the time variation of the heat flux. Typically, a window of 160 × 128 pixels, allowing for a frame rate at 1.25 kfps, is used to estimate the wall heat flux q_w.

Droplet temperature measurements using 2cLIF thermometry

The measurements of the droplet temperature reported in this study were obtained using exactly the same method as described by Chaze et al. [17]. More details concerning the optical setup and the selection of temperature-sensitive fluorescent dyes can be found in Chaze et al. [17,19]. A pulsed Nd:YAG laser (Quantel Bril-

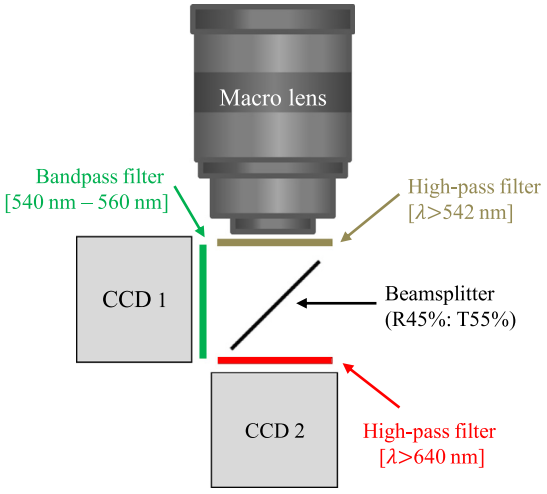

Fig. 4. Optical detection system used in the 2cLIF imaging technique.

lant B @532 nm, up to 450 mJ per pulse) is utilized for the excitation of a mixture of two fluorescent dyes, namely sulforhodamine 640 (SR640) and disodium fluorescein (FL), which are dissolved into water prior to the drop generation. The fluorescence signal of FL increases with temperature (about 3%/°C) due to the increase of its absorption cross section at the laser wavelength [19]. The fluorescent emission of SR640 does not vary with temperature and is red-shifted by a few tens of nm compared to FL. As displayed in Fig. 4, droplets are observed by means of two CCD cameras (Allied Vision Tech Prosilica GT3300 B/C GigE Camera 3296 × 2472, 12 bits, 5.5 µm) each one equipped with an interference filter for the detection of the fluorescence in the bands indicated in Fig. 4. The optical system also includes an objective lens (SIGMA APO MACRO 150 mm F2.8 EX DG OS HSM and its teleconverter ×2) and a beamsplitter mounted in front of the cameras. A high pass filter ($\lambda > 542$ nm) is added between the objective lens and the beamsplitter to eliminate more efficiently the scattered laser light. Calculating the pixel-to-pixel ratio of the images recorded by the two cameras allows eliminating disturbances affecting the signal intensity. In particular, it eliminates the effect of the droplet deformation, since the fluorescence signal in the two detection bands is affected almost identically by light scattering at the droplet surface. Finally, the fluorescence ratio is converted into temperature with use of a calibration performed apart in a glass cuvette where the same liquid solution is controlled in temperature. The repetition rate of the pulsed laser (f=10 Hz) is too low to resolve temporally the impact process which occurs within a few ms. A time reconstruction of the heating process is done by shifting the laser pulse in respect to the detection of the falling droplet by the optical barrier. Two configurations of the optical system are used to visualize the impacting droplet (Fig. 5). A 45° tilted mirror is placed under the sapphire window and its heated holder. It makes it possible to observe the droplet from below with the cameras, while a side illumination by the laser is performed (Fig. 5a). The same mirror can also be used to illuminate the droplet from below, while the cameras are taking side view images of the droplet (Fig. 5b). Although the concentration of both dyes is low (C_{FL}=2.10^{-4} M and C_{SR640}=0.7·10^{-6} M), an effect of the dye on the surface tension is not excluded, but no significant change in the spreading diameter was observed compared to droplets of pure water [4,20].

3. Boiling regimes

Depending on this initial wall temperature, two types of pattern can be evidenced on the IR images as illustrated in Fig. 6. There are strong similarities with the TIR images presented by Khavari et al. [14] in the case of ethanol droplets. For T_{w0} > 450°C, a fingering pattern can be clearly observed. The boiling regime below 450°C corresponds to the bubbly boiling regime in Fig. 1(a). In addition to the formation of fingers, the transition between the two boiling regimes is marked by a change in the area of effective heat transfer, especially for We=92.

3.1. *Bubbly boiling*

In this situation of transition boiling, the liquid lamella can be divided into two regions [21,22] as shown in Fig. 7(a). A wetting contact with the wall is observed at the center (with several nucleation spots and bubbles), while the edge of the lamella is lifted from the substrate. Due to the vapor layer separating the droplet and the solid surface, the heat transfer is much less intense in the edge region. This is illustrated in Fig. 7(b) and (c) which shows measurements of the liquid temperature in the drop T_l and the wall heat flux q_w for We=92 and T_{w0}= 400°C. The lifted edge of the liquid lamella displays an higher temperature, while the wall heat flux q_w is the most intense in the central wetted region. For We=92, the radius of the wetted area R_w (red dotted line) is getting significantly smaller than the spreading radius R_s (black dotted line) during the impact process.

For more details, Fig. 8(a) and (b) present the time evolution of the liquid temperature in the drop T_l, the solid surface temperature

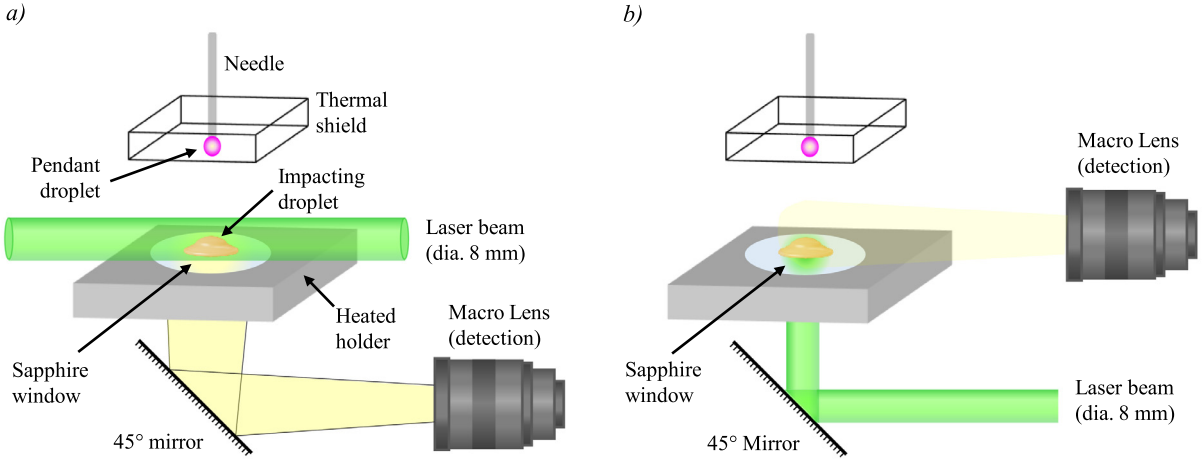

Fig. 5. The two optical configurations used to visualize the fluorescence emission of the impinging droplet (a: bottom view imaging, b: side view imaging).

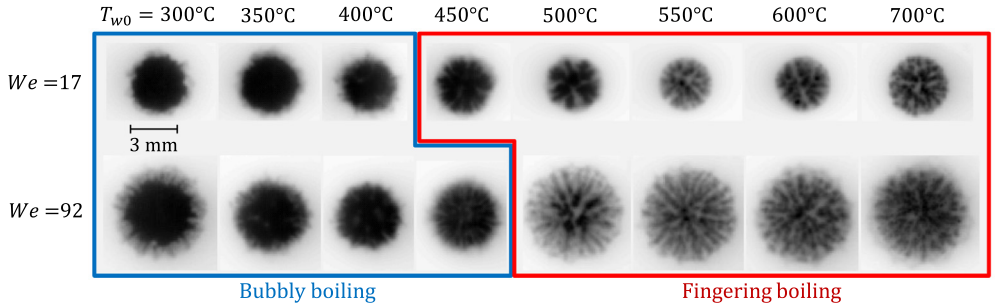

Fig. 6. IR images illustrating the change of the thermal footprint of the droplet in the Leidenfrost transition. These images corresponds to a time of about 3 ms after the beginning of the drop impact and d_0=2.6 mm.

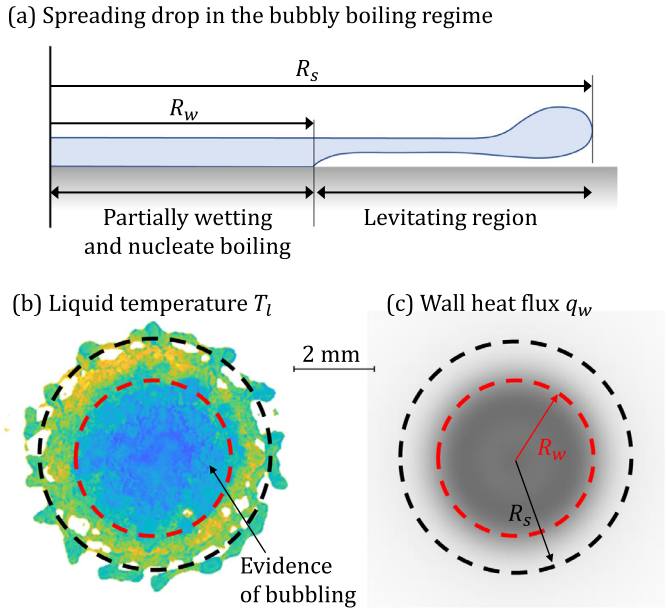

Fig. 7. Illustration of the bubbly boiling regime by a schematic of the spreading droplet (a) and the distributions of the liquid temperature in the drop (b) and the wall heat flux (c) characterized experimentally for *We*=92 and *t*=2 ms. The scale bar of 2 mm applies to figures (b) and (c).

T_S and the wall heat flux q_w for *We*=30 and *We*=92 at T_{w0}=400°C. Immediately after the beginning of the impact, the liquid in contact with the solid surface becomes superheated. This cannot be observed in the 2cLIF images, as the temperature measurements result from the integration of the fluorescence signal over the entire thickness of the droplet in the line of sight of the detector. A short time after the first contact of the liquid with the wall (typically a few μs), vapor bubbles appear at multiple nucleation spots on the solid surface. Vapor bubbles grow and eventually form dry patches on the wall surface which locally reduces the heat flux. Despite the limited pixel resolution of the IR images, some of these dry patches or bubbles can be pointed out. They can be also evidenced on the LIF images of the liquid temperature where they form patches of slightly lower temperature (especially at 1.5 ms for *We*=92 and 2 ms for *We*=30). One of the possible explanation is that the presence of bubbles locally reduce the thickness of the liquid illuminated by the laser and push superheated liquid away from the solid surface, which can make those bubbles somehow visible on the 2cLIF images.

During the drop spreading, the liquid lamella breaks up because of the expansion of several holes. For *We*=92, the hole opening occurs at *t*=1.5 ms. Multiple holes are present on the drop periphery where the lamella is the thinnest. The holes expand towards the center of the lamella with a retracting velocity driven by capillary forces [23]. For *We*=30, the formation of holes takes a longer time, because the lamella thining occurs at a slower pace during the spreading (see Eq. 27) and bubbles must have a size comparable to the lamella thickness to induce the opening of a hole.

Not visible in Fig. 8, but on the sideview images by Khavari et al. [14] in Fig. 1a, an intensive thermal atomization occurs when bubbles reach the upper surface of the lamella and burst. This phenomenon has been extensively described in different studies such as Cossali et al. [24] and Roisman et al. [21].

3.2. *Fingering boiling*

IR measurements reveal that there is no wetting contact at the wall temperatures associated with fingering boiling in the case of water contrary to ethanol droplets [14]. When fingers are present, the surface temperature never falls below the spinodal temperature of water $T_{spin} \approx 320$°C (Fig. 17). Figs. 9 and 10 show typical evolution of the liquid temperature at T_{w0}=600°C. Fingering can be noticed at *t*=2 ms and *t*=3 ms for *We*=92. In the absence of bubbling and wetting, the breakup takes place much later than in the bubbly boiling regime. For *We*=92, the time of the breakup is roughly 3–4 ms at T_{w0}=400°C against 7 ms at T_{w0}=600°C. The breakup is driven by an instability of the rim edging the droplet. The size of the liquid protrusions that appear on the rim, increases with time, which eventually leads to the rupture of the rim. For *We*=30, the growth of this instability is very slow, allowing the bouncing of the droplet. Although the opening of the lamella still occurs for *We*=92, there is usually no more than one or two holes propagating. They are observed later in the impact process, when the liquid lamella is so thin that a very small disturbance is enough to create a hole. This never happens in the case of *We*=30, because the spreading is limited and the lamella never gets thin enough. For the bubbly boiling regime in Fig. 8, bubbles of a significant size are able to open the lamella even for the low *We* and at an earlier time, when the lamella is still relatively thick (typically, the thickness of the lamella decreases as $1/t^2$ as shown in Eq. 27).

The overall heating of the liquid is less important than in the bubbly boiling. In the case of *We*=30, the heating of the liquid is almost twice as low. Liquid fragments leave the wall surface at a much higher temperature in the case of *We*=92. This can be attributed to the drop spreading and the subsequent increase in the surface area for heat transfer. The spreading diameter is more important for *We*=92. In fact, the situation is more complex as the lamella becomes very thin for the large *We*, its capacity to absorb heat is reduced. This will be discussed more in details in Section 5.

Description of the fingering To further examine the fingers, IR images are recorded with an enhanced resolution of 512 × 512

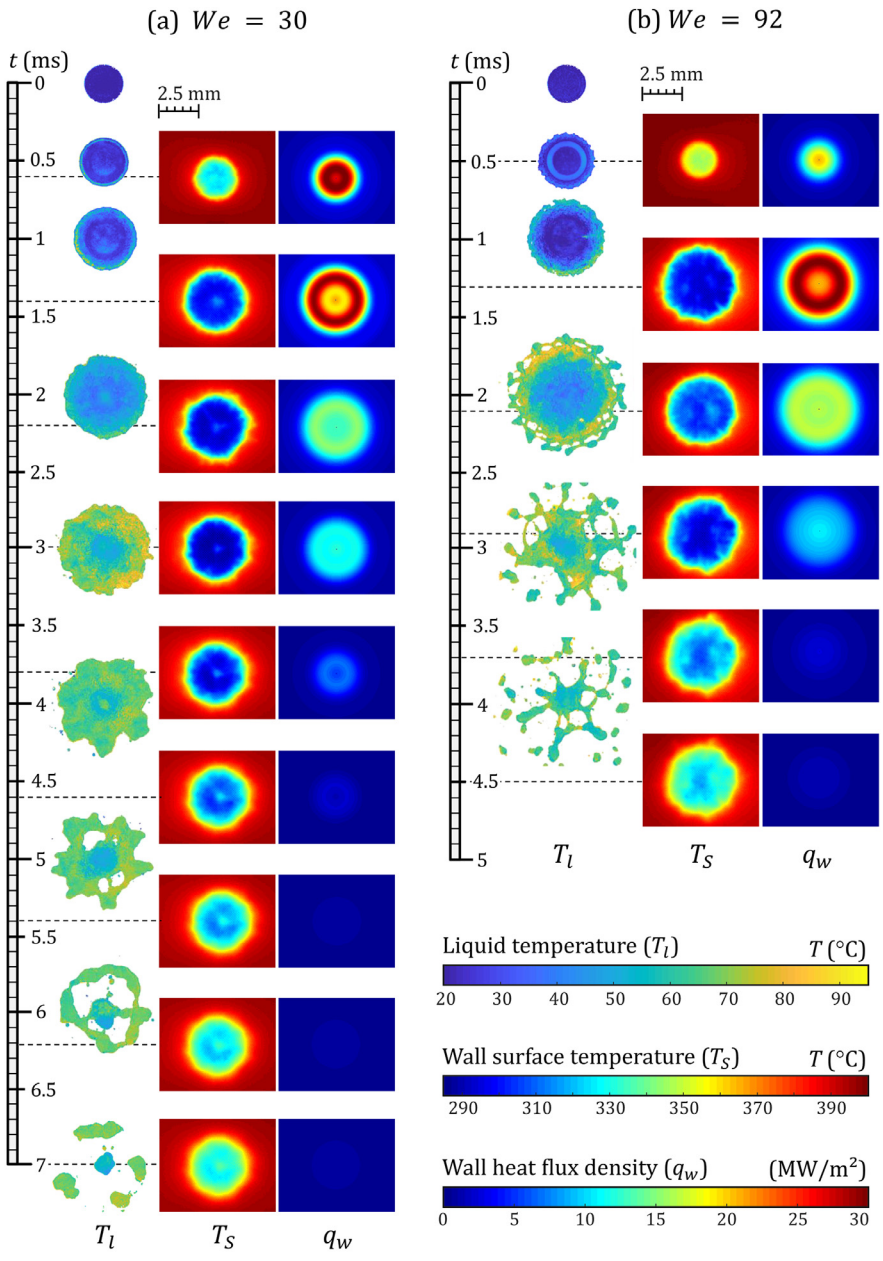

Fig. 8. Heat transfer at the drop impact onto the sapphire substrate at T_{w0}=400°C. Images show the liquid temperature in the drop T_l, the surface temperature of the substrate T_S and the reconstructed distribution of the heat flux at the solid surface q_w for *We*=30 (a) and *We*=92 (b).

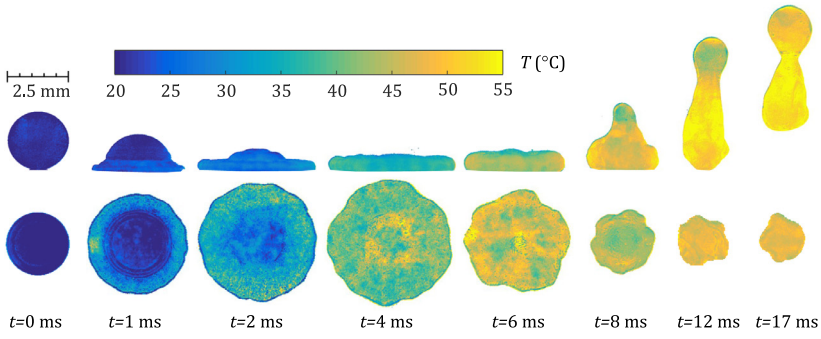

Fig. 9. Side and bottom views of the temperature field within an impacting droplet at *We*=30 and T_{w0}=600°C.

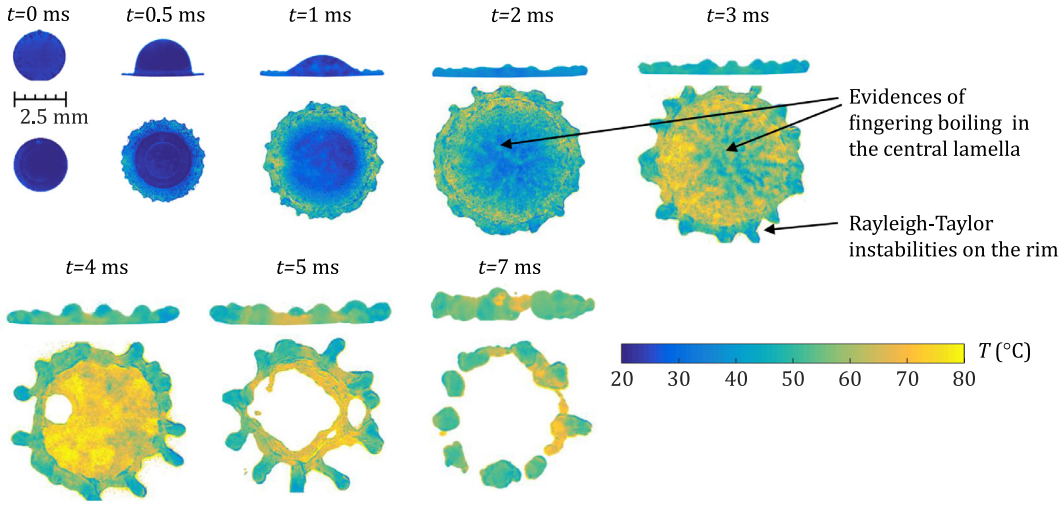

Fig. 10. Side and bottom views of the temperature field within an impacting droplet at We=92 and T_{w0}=600°C.

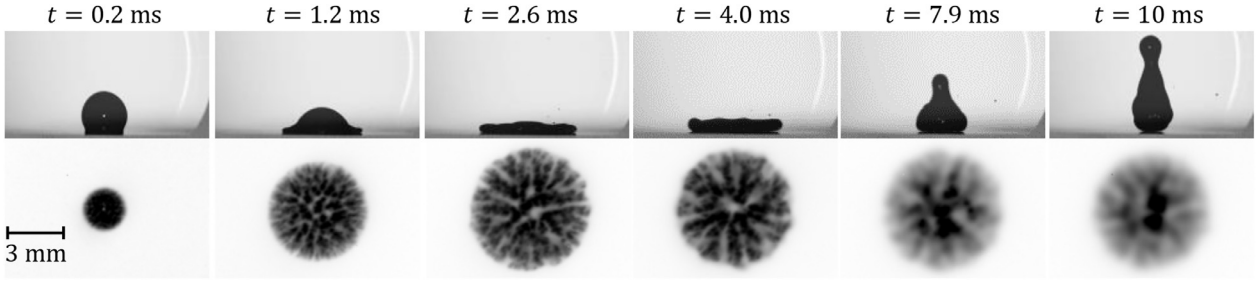

Fig. 11. Time evolution of the fingering pattern for We=30 at T_{w0}=600°C.

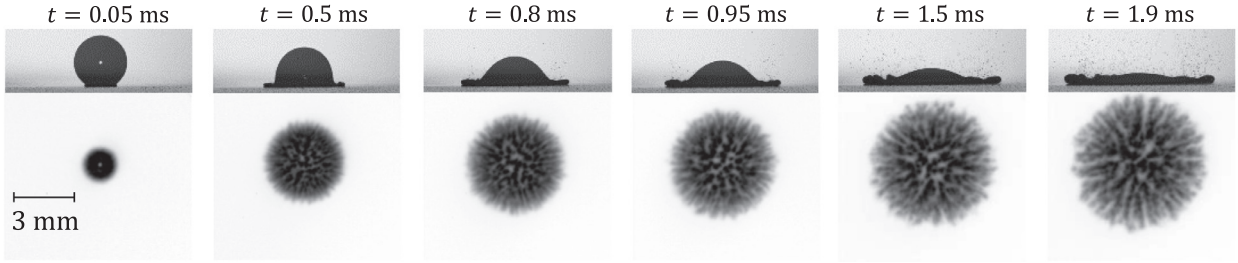

Fig. 12. Time evolution of the fingering pattern for We=64 at T_{w0}=600°C.

pixels. The acquisition rate is only 200 fps at this resolution, so no more than two images can be recorded per drop impact. Drop impacts are repeated several times and the camera trigger is time-shifted with respect to the drop impact using the optical barrier. This rather cumbersome approach for reconstructing the time evolution of the fingering pattern was only applied for a limited number of cases at T_{w0}=600°C (Figs. 11 and 12). The acquisitions are also synchronized with a high-speed camera to obtain sideview images of the impinging drops in shadowgraphy. The latter reveals the existence of tiny droplets ejected upward from the edge of the lamella in the case of We=64 but not We=30. This form of secondary atomization has been already reported by Tran et al. [4] who referred to 'spraying film boiling' and it is only visible when increasing We as the lamella is getting thinner during the spreading process.

Infrared images in Figs. 11 and 12 reveal a branching structure for the fingering pattern. To determine the number N of fingers, IR images are first rewrapped in the polar coordinates (r, θ) with r the radial distance to the drop center and θ the azimuth angle (Fig. 13). Then, local minima and maxima of digital levels are detected for a given value of r in order to assess N. The result of this detection is presented in Fig. 13 for We=30 and t=2.4 ms. N is roughly proportional to r as it appears in Fig. 13 (c). Further analyses also show that the ratio N/r scales as $t^{-0.3}$ (Fig. 14). After the droplet has reached its maximum spreading, the thermal footprint progressively becomes blurred due to the thermal relaxation by heat conduction in the solid substrate, subsequent to the receding and break-up of the droplet. For this reason, the detection of the fingers was restricted to the spreading phase in Fig. 14.

Fig. 15 presents several radial profiles of N (number of fingers at a fixed distance r) for different We. The value of N is not influenced by the impact velocity. This may appear in contradiction with the observations of Khavari et al. [14], who noted an increase in the number of fingers with We. However, Khavari et al. [14] accounted for the number of fingers on the droplet edge (and most likely at the maximum spreading). Based on the above description of the fingering pattern, the number of fingers N_{max} on the drop periphery at the time of maximum spreading t_{max}, can be evaluated by:

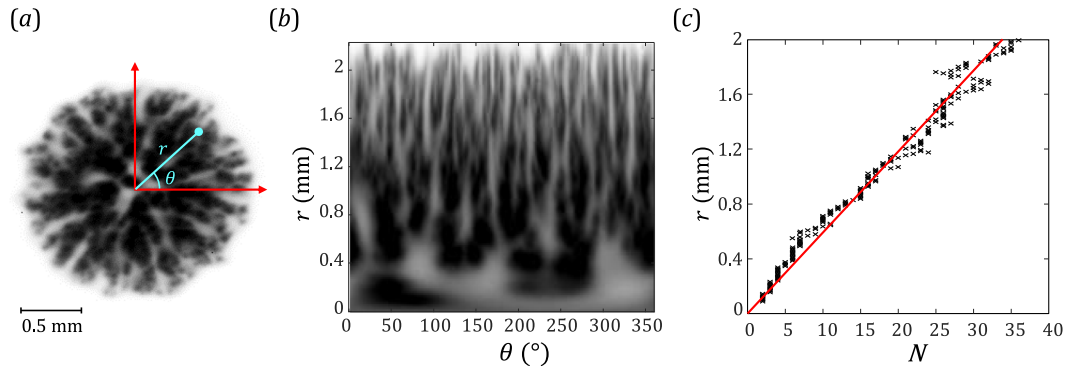

Fig. 13. Illustration of the image processing to determine the number of fingers N in the case We=30 at t=2.3 ms and T_{w0}=400°C. The raw IR image is first rewrapped in the polar coordinates (r, θ) (b), then the number N of local maxima at a fixed radius r is determined (c).

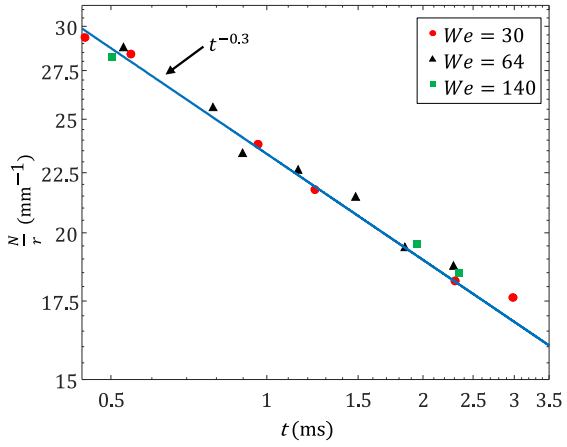

Fig. 14. Influence of the time t on the number of fingers N. The ratio N/r decreases with time as $t^{-0.3}$ during the drop spreading. Experimental data obtained at T_{w0}=600°C.

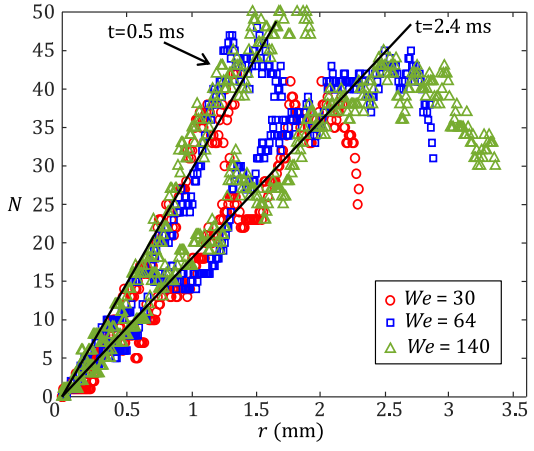

Fig. 15. Influence of We on the number of fingers N. At given r and t, the number N of fingers is not influenced by We. Experimental data obtained at T_{w0}=600°C.

$$N_{max} \sim d_{max} \cdot t_{max}{}^{-0.3}, \quad (1)$$

where $d_{\max}$ is the maximum spreading diameter. According to Tran et al. [4], $d_{\max} \sim We^{0.39}$ for $We > 10$ in the case of water. On the other hand, $t_{\max}$ slightly decreases with We. Based on the experimental data of Castanet et al. [20, see Fig. 13 page 16], an acceptable scaling for $t_{\max}$ is given by:

$$t_{max} \sim t_\gamma \cdot We^{-0.15}, \quad (2)$$

where $t_\gamma = \pi/4\sqrt{\rho d_0^3/\gamma}$ is the Rayleigh oscillation time. In the current experiments, d_0 remains equal to 2.6 mm and so t_γ is a constant. Using Eqs. (1) and (2), it is expected that:

$$N_{max} \sim We^{0.44}. \quad (3)$$

Fig. 16 shows the evolution of $N_{\max}$ as a function of We. The results concern water but also ethanol based on the data provided by Khavari et al. [14]. Eq. (3) is in good agreement with results obtained for both liquids. It should be noticed that the effect of We on $d_{\max}$ and $t_{\max}$ are about the same for water and ethanol [20, see Figs. 9 and 13]. Finally, the major difference with ethanol concerns the effect of the wall temperature on the fingering. For ethanol, the fingering pattern is observed in a narrow range of temperature between 200°C and 260°C by Khavari et al. [14]. A recent work by Castanet et al. [16] confirms the absence of fingers for ethanol above T_{w0}=300°C using the same IR technique as in the present study. Khavari et al. [14] also noticed that the number of fingers is decreasing with T_{w0}. In our experiments, the temperature of the solid substrate was limited to T_{w0}= 700°C. At this temperature, fingers are still present and their number is not significantly different from 600°C.

4. Leidenfrost point and liquid superheating

When a drop impinges on the hot substrate, the surface temperature of the substrate T_S first decreases. It reaches a minimum $T_{S,min}$, then it eventually returns to the initial wall temperature T_{w0}. Fig. 17 shows the variation of $T_{S,min}$ as a function of T_{w0}. The impingement of a water droplet on a superheated sapphire substrate has been already studied by Tran et al. [4], who examined the Leidenfrost transition based on sideview images of the impact. They located the onset of film boiling at about 450°C for We in the order of a few tens. The observation of Tran et al. [4] are congruent with the present results. Fingers can be observed at T_{w0}=450°C for We=17, but a slight increase of the wall temperature is required for their formation at higher We. As expected, $T_{S,min}$ never goes below the spinodal temperature $T_{spin} \approx$ 320°C in the film boiling regime (ie. for $T_{w0} >$ 450°C). The LFP corresponds to an initial wall temperature $T_{w0} \approx$ 450°C, for which it is observed that $T_{S,min}$ is about equal to T_{spin}. This means that it is the highest conceivable value of the LFP that is actually achieved in these drop impacts.

4.1. Theoretical description of the thermal contact

When two semi-infinite bodies initially at temperature T_1 and T_2 are brought in perfect thermal contact, the temperature at the

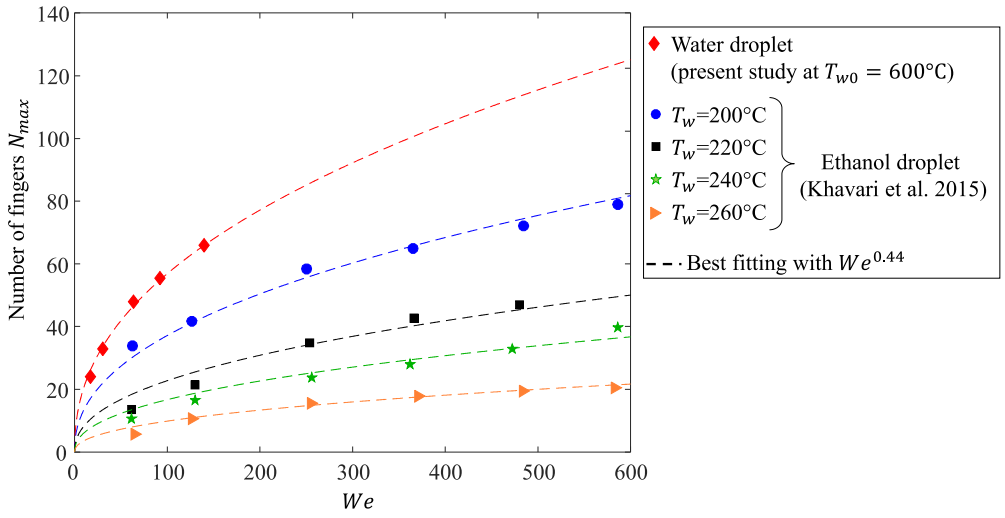

Fig. 16. Maximum number of fingers N_{max} on the droplet edge during the drop spreading. Results for water are extracted from IR images having a resolution of 160 × 128 pixels. This allows including data from more experimental cases, but reduces the value of N_{max} compared to the results presented in Figs. 13 to 15.

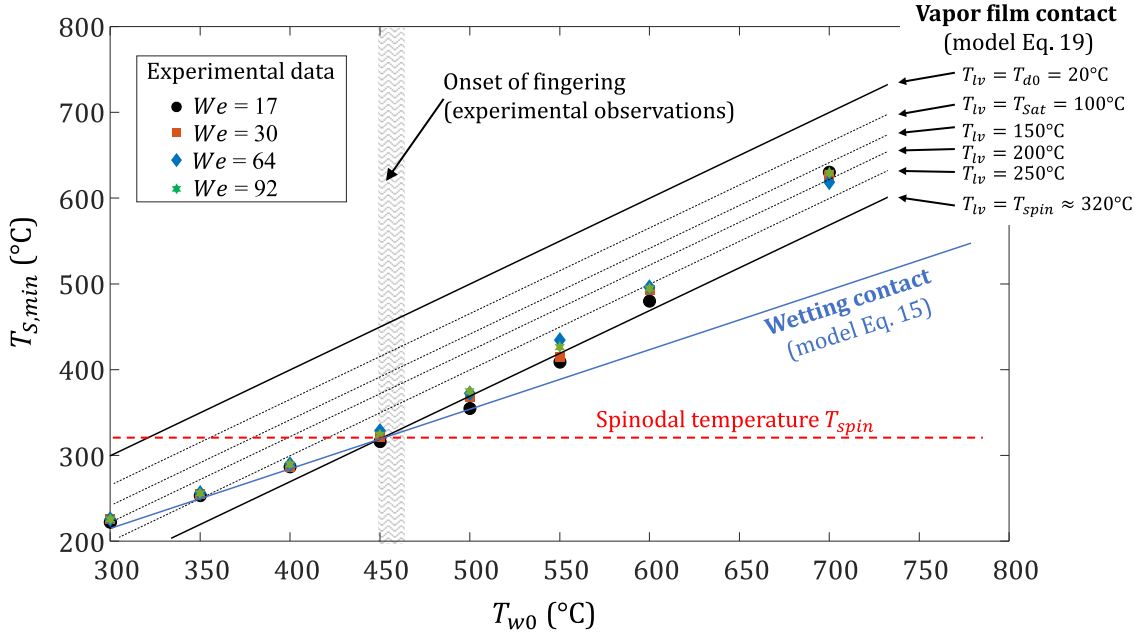

Fig. 17. Maximal decrease in temperature of the solid surface during the impact process for different *We*.

contact surface T_c instantly takes a value that is determined by their respective thermal effusivities e_1 and e_2:

$$T_c = \frac{e_1 T_1 + e_2 T_2}{e_1 + e_2}. \tag{4}$$

This expression for the contact temperature is valid at any time in the case of two semi-infinite bodies. Eq. (4) which assumes that heat transfer is only of conducive nature, is also a good approximation for the contact temperature of finite bodies. In that case, it is valid near the center of the contact region, as long as the thermal diffusion length remains small in comparison to the thickness of the bodies and to the dimensions of the contact area. Eq. (4) implicitly assumes that the heat transfer is purely by heat conduction in the two bodies. Therefore, this equation does not directly applied to the case of a spreading drop, where the internal liquid flow intensifies the heat transfer by convection and reduces the thickness of the thermal boundary layer developing in the liquid lamella [16,25]. As detailed by Breitenbach et al. [25], the temperature field resulting from the contact with a spreading drop can be approximately described by solving a one-dimensional heat equation in the liquid and solid phases separately. The heat equation in the liquid and solid phases can be expressed as:

$$\frac{\partial T_l}{\partial t} + u_z \frac{\partial T_l}{\partial z} = \alpha_l \frac{\partial^2 T_l}{\partial z^2}, \tag{5}$$

$$\frac{\partial T_w}{\partial t} = \alpha_w \frac{\partial^2 T_w}{\partial z^2}, \tag{6}$$

where u_z is the vertical component of the liquid velocity. The heat transfer in the r direction is neglected, which is valid close to the contact interfaces. In the liquid phase, the following non-viscous solution can be considered for the velocity field [26]:

$$u_r = r/t, \quad u_z = 2z/t. \tag{7}$$

The above equation is a good approximation for the velocity field provided sufficiently large values of *We* and *Re* (typically *We* > 10

and $Re > 100$). A self-similar solution to Eqs. (5) and (6) can be obtained by the introduction of a similarity variable $\xi = z/\sqrt{\alpha t}$ with α=α_l or α_w. This yields an ordinary differential equation for the temperature fields $T_l(\xi)$ and $T_w(\xi)$:

$$T_l'' + \frac{5}{2}\,\xi\,T_l' = 0, \tag{8}$$

$$T_w'' + \frac{1}{2}\,\xi\,T_w' = 0. \tag{9}$$

A constant and uniform temperature T_c at the contact surface can be considered for the boundary conditions at the liquid or solid interfaces located at ξ=0:

$$T_l = T_c \text{ at } \xi = 0, \qquad T_l = T_{d0} \text{ at } \xi = \infty, \tag{10}$$

$$T_w = T_c \text{ at } \xi = 0, \qquad T_w = T_{w0} \text{ at } \xi = \infty. \tag{11}$$

The similarity solutions of Eqs. (8) and (9) are respectively:

$$T_l(z,t) = T_c + (T_{d0} - T_c)\,erf\left(\frac{\sqrt{5}\,z}{2\sqrt{\alpha_l t}}\right), \tag{12}$$

$$T_w(z,t) = T_c + (T_{w0} - T_c)\,erf\left(\frac{z}{2\sqrt{\alpha_w t}}\right), \tag{13}$$

where $e_l = \sqrt{\rho_l Cp_l \kappa_l}$ and $e_w = \sqrt{\rho_w Cp_w \kappa_w}$ are the effusivity of the liquid and the solid substrate. From the above solutions, the heat flux at the contact surface, can be determined by :

$$q_l(t) \equiv \kappa_l \left.\frac{\partial T_l}{\partial z}\right|_{z=0} = \frac{\sqrt{5}\,e_l\,(T_c - T_{d0})}{\sqrt{\pi t}}, \tag{14}$$

$$q_w(t) \equiv -\kappa_w \left.\frac{\partial T_w}{\partial z}\right|_{z=0} = \frac{e_w\,(T_{w0} - T_c)}{\sqrt{\pi t}}, \tag{15}$$

where T_{d0} and T_{w0} are respectively the temperatures of the droplet and the solid substrate prior to the contact. The factor $\sqrt{5}$ in Eq. (14) takes into account the enhancement of heat transfer induced by convection in the spreading lamella.

4.2. Thermal contact in the partially-wetting boiling regime

When there is a wetting contact between the droplet and the solid surface, the surface temperature rapidly reaches a minimum value $T_{S,min}$ at the center of the impact region. The temperature at this location remains about constant for a few ms. Eventually, it rises and returns to T_{w0} due to the fact that the droplet is not a semi-infinite body. Neglecting the contribution of liquid vaporization to the cooling (this approximation will be justified later in Section 5 based on experimental measurements), the temperature of the wetting contact can be obtained by equating the expressions of q_l and q_w in Eqs. (14) and (15),

$$T_c = \frac{\sqrt{5}\;e_l\,T_{d0} + e_w\,T_{w0}}{\sqrt{5}\;e_l + e_w}. \tag{16}$$

As T_{w0} increases, the liquid in contact with the solid substrate is more and more superheated. The above expression of T_c is plotted as a blue line in Fig. 17. It perfectly matches the experimental data for the minimum temperature of the surface $T_{S,min}$, until T_{w0} reaches the LFP.

4.3. The Leidenfrost point

Basically, no wetting is possible if the temperature of the solid surface remains above the spinodal temperature T_{spin} during the cooling process. In the scenario considered below, the rapidity of the contact is such, that the liquid temperature reaches the maximum conceivable value (i.e. the spinodal point T_{spin}). This implies a sufficiently large impact velocity, since the dynamics of the lubrication layer of gas are extremely important at low velocities (Even a drop deposited on an unheated surface can glide on a trapped air cushion at low impact velocities [27]). Assuming $T_{S,min}$ is equal to T_{spin} in the followings, it is possible to obtain an expression for the dynamic LFP. Using Eq. (16), we can write:

$$T_c = T_{spin} = \frac{\sqrt{5}\;e_l\,T_{d0} + e_w\,LFP}{\sqrt{5}\;e_l + e_w}. \tag{17}$$

From this expression, the dynamic LFP can be determined by:

$$LFP = T_{spin} + f(We, Re)\cdot\frac{e_l}{e_w}\cdot\left(T_{spin} - T_{d0}\right), \tag{18}$$

where $f = \sqrt{5}$ for the non-viscous velocity field in Eq. (7). Considering κ_w=14 W.m^{-1}.K^{-1}, Cp_w=1150 J.kg^{-1}.K^{-1} and ρ_w=3980 kg.m^{-3} for the thermal properties of sapphire, e_w is about 8000 J.K^{-1}.m^{-2}.s$^{-1/2}$. For water, κ_l=0.6 W.m^{-1}.K^{-1}, Cp_w=4180 J.kg^{-1}.K^{-1} and ρ_w=1000 kg.m^{-3}, which yields e_l=1580 J.K^{-1}.m^{-2}.s$^{-1/2}$. Applying Eq. (18), the LFP is about 453°C, which is consistent with the experimental observations (evidence of the onset of the fingering boiling). According to Eq. (18), the liquid subcooling T_{Sat}–T_{d0} has a weak influence on LFP, since T_{d0} is small compared to T_{spin}. This trend is also in good agreement with the literature [7]. The velocity field in Eq. (7) is only valid for relatively large impact velocities, when liquid inertia is predominant over viscous and capillary forces. Typically, *We* has to be in the range of 10, while *Re* has to be of a few hundreds[28]. For the low impact velocities, it can be anticipated that f takes a smaller value tending towards 1 when U_0 is approaching 0. This corresponds to a LFP tending toward 380°C according to Eq. (18). This agrees well with the results of Tran et al. [4], who found a dynamic LFP close to 380°C for *We*=4. Hence, Eq. (18) seems to hold for this relatively low value of *We*. However, Eq. (18) does not apply to a sessile droplet. It largely overestimates the static LFP (about 220°C according to [4]). In the case of the sessile drop, a superheating of the liquid is not conceivable. The sessile droplet remains in a thermal equilibrium, meaning that its temperature is equal to T_{Sat}.

4.4. Liquid superheating in the film boiling regime

In the film boiling regime, Eq. (14) can be modified to determine the heat flux q_l entering into the droplet. The temperature T_c in Eq. (14) is replaced by T_{lv} the temperature at the liquid/vapor interface, which leads to:

$$q_l = \frac{\sqrt{5}\,e_l\,(T_{lv} - T_{d0})}{\sqrt{\pi t}}. \tag{19}$$

This equation implies that the temperature of the liquid/vapor interface T_{lv} remains approximately constant during the impact process. This assumption is made in almost all the models for the film boiling, which presumes that T_{lv}=T_{Sat}. Equating the expressions of q_l and q_w, and replacing T_c by T_{lv} on the liquid side, one obtains:

$$\frac{\sqrt{5}\,e_l\,(T_{lv} - T_{d0})}{\sqrt{\pi t}} = \frac{e_w\,(T_{w0} - T_c)}{\sqrt{\pi t}}. \tag{20}$$

This equation can be used to determine the contact temperature T_c at the solid surface, which is expected to compare with $T_{S,min}$:

$$T_{S,min} = T_c = T_{w0} - \sqrt{5}\cdot\frac{e_l}{e_w}\cdot(T_{lv} - T_{d0}). \tag{21}$$

The surface temperature $T_{S,min}$ determined by Eq. (21) is plotted in Fig. 17 as a function of T_{w0}. These are parallel lines that are shifted vertically for each value of T_{lv} being considered. In most of the models for the film boiling, it is assumed that T_{lv}=T_{Sat} [16,25]. However, with this assumption, the cooling of the solid surface is by far too small in comparison with the experiments. To have a better agreement, it is necessary to consider that the liquid/vapor interface can be largely superheated in the film boiling regime. Until T_{w0}=550°C, T_{lv} remains about equal to T_{spin}. Then, increasing T_{w0}, the superheating of the liquid/vapor interface becomes less and less important. At T_{w0}=700°C, T_{lv} is still about 200°C. Presumably, it would have been necessary to raise the wall temperature to a much higher value in order to have actually T_{lv} equal to T_{Sat}.

The above description suggests that the fingering boiling is in fact a form of homogeneous nucleation. At the very beginning of impact, the liquid is heated so strongly in a small layer of liquid close to the liquid/vapor interface, that it becomes superheated. This permits the formation of numerous vapor bubbles by homogeneous nucleation. The liquid layer where homogeneous nucleation occurs, is very thin (typically just a few μm), because its thickness must remain small in comparison to that of the thermal boundary layer h_t which evolves as $h_t \sim \sqrt{\alpha_l t}$. The vapor bubbles are then transported by the liquid flow. This transport is more efficient than in the case of bubbly boiling and heterogeneous nucleation. It is not restrained by the pinning of triple contact lines (bubbles attached on the solid surface). During their transport, the vapor bubbles undergo an elongation in the radial direction, since the velocity field in Eq. (7) corresponds to a uniform strain rate along the radial direction. The growth and elongation of the bubbles accelerates the process of bubble coalescence, which results in the formation of separated fingers. The vapor is mainly conveyed to the edge of the spreading drop by flowing into the ridges that separate the fingers. Considering that nucleation is uniformly distributed at the liquid/vapor interface, it is expected that the number of fingers N increases proportionally to r as observed experimentally. Since the liquid superheat decreases with T_{w0} (Fig. 17), N is also expected to decline with T_{w0} as described by Khavari et al. [14]. However, only the larger fingers can be seen experimentally. While the rate of homogeneous nucleation increases with the liquid superheat, the initial size of the nuclei decreases inversely. It should be noted that the formation of very fine bubbles by homogeneous nucleation above the LFP is also evidenced by the ejection of very fine droplets (Fig. 12). This phenomenon corresponds to the 'spraying film boiling' extensively described by Tran et al. [4]. Some of the vapor bubbles can find a way through the lamella which is very thin on the edge of the spreading droplet.

In the case of ethanol, the spinodal temperature is about 213°C [29]. Fingers can be observed starting from $T_{w0} \approx 200$°C [14]. Given the low thermal effusivity of liquid ethanol (e_l=560 J.K^{-1}.m^{-2}.s$^{-1/2}$) compared to sapphire, the contact temperature T_c does not decrease below T_{w0} by more than a few °C during the cooling process. The superheating of liquid ethanol is therefore very significant. Applying Eq. (18) with $f = \sqrt{5}$ leads to an LFP of approximately 240°C. Fingers are not observed by both the TIR method and IR thermography techniques for $T_{w0} > 270$°C. Castanet et al. [16] studied the time evolution of the vapor film thickness of ethanol droplets using IR thermography starting from T_{w0}=300°C and they did not observe fingering boiling. In this study, it is worth noting that T_{lv} could be assumed equal to T_{Sat} to describe the heat transfer and the evolution of the vapor film thickness. The superheating of the liquid seems to have disappeared, probably because the thickness of the vapour film gets larger while increasing T_{w0}. The vapor film thickness reaches more than 10 μm during the impact process at T_{w0}=300°C [16]. In comparison, the film thickness is of the order of 1 μm in the case of water at T_{w0}=600°C as determined by Chaze et al. [15].

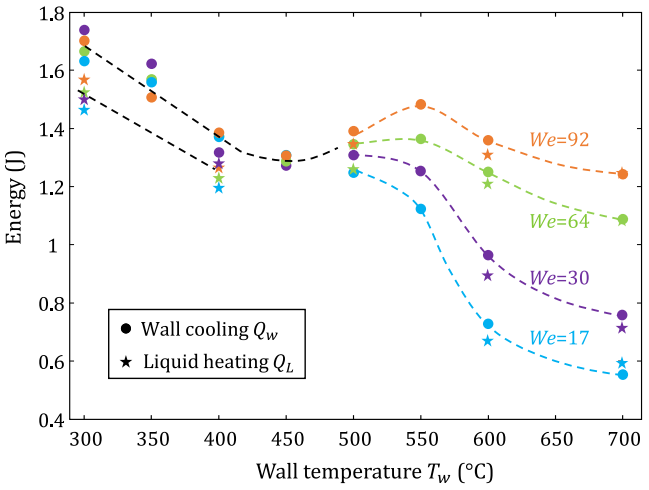

Fig. 18. Experimental data showing the evolution of the heat taken from the solid surface Q_w and the heat transferred to the liquid Q_l as a function of the wall temperature T_{w0}. The overall accuracy of the measurements is about 0.1 J for both Q_l and Q_w. The smooth curves with dotted lines are introduced here to highlight trends in these experimental data.

5. Heat transfer in the Leidenfrost transition

5.1. Heat transfer characteristics

In the following section, the emphasis is placed on the heat transfer characteristics associated with the drop impact. The heat taken to the wall (Q_w) can be determined by integrating the local heat flux q_w over time and space. An axisymmetric distribution is assumed for q_w when solving the inverse heat conduction problem in the sapphire substrate [15], thus it can be written:

$$Q_w = 2\pi \int_{t=0}^{\infty} \int_{r=0}^{\infty} q_w(r,t) r \, dr \, dt. \tag{22}$$

The heat gained by the liquid (Q_l) can be evaluated from the temperature of the liquid fragments measured by 2cLIF. Due to the short duration of the droplet/wall interaction (typically a few ms), the mass of evaporated liquid can be neglected [16]. Therefore, Q_l can be evaluated as follows:

$$Q_l = m \, Cp_l (T_m - T_{d0}), \tag{23}$$

where m is the mass of the drop, T_m is the average temperature of the outcoming liquid determined from the 2cLIF images. It is calculated doing the arithmetic average of the temperature field in the 2cLIF images. T_{d0} is the initial temperature of the drop. Fig. 18 shows the evolution of Q_w and Q_l as a function of the initial wall temperature T_{w0} for different *We*. Several comments can be made from this figure:

- In the bubbly boiling regime (from 300°C to 450°C), both Q_l and Q_w are decreasing with T_{w0}. This is mainly because an increasing fraction of the lamella at the periphery of the drop is levitated over a vapor film, which acts as an thermal insulator. The heat transfer is weakly dependent on *We* in this range of wall temperature.
- In the fingering film boiling regime ($T_{w0} > 450$°C), the heat transfer (Q_l and Q_w) decreases again with T_{w0}. A clear separation of the curves for the different *We* can also be noticed above T_{w0}=500°C.
- In the bubbly boiling regime, Q_l is slightly lower than Q_w. The small difference between Q_w and Q_l is not exclusively the result of the contribution of liquid vaporization ($Q_{vap} = Q_w - Q_l$). Thermal atomization produces numerous tiny secondary droplets that are too small to be visualized by fluorescence

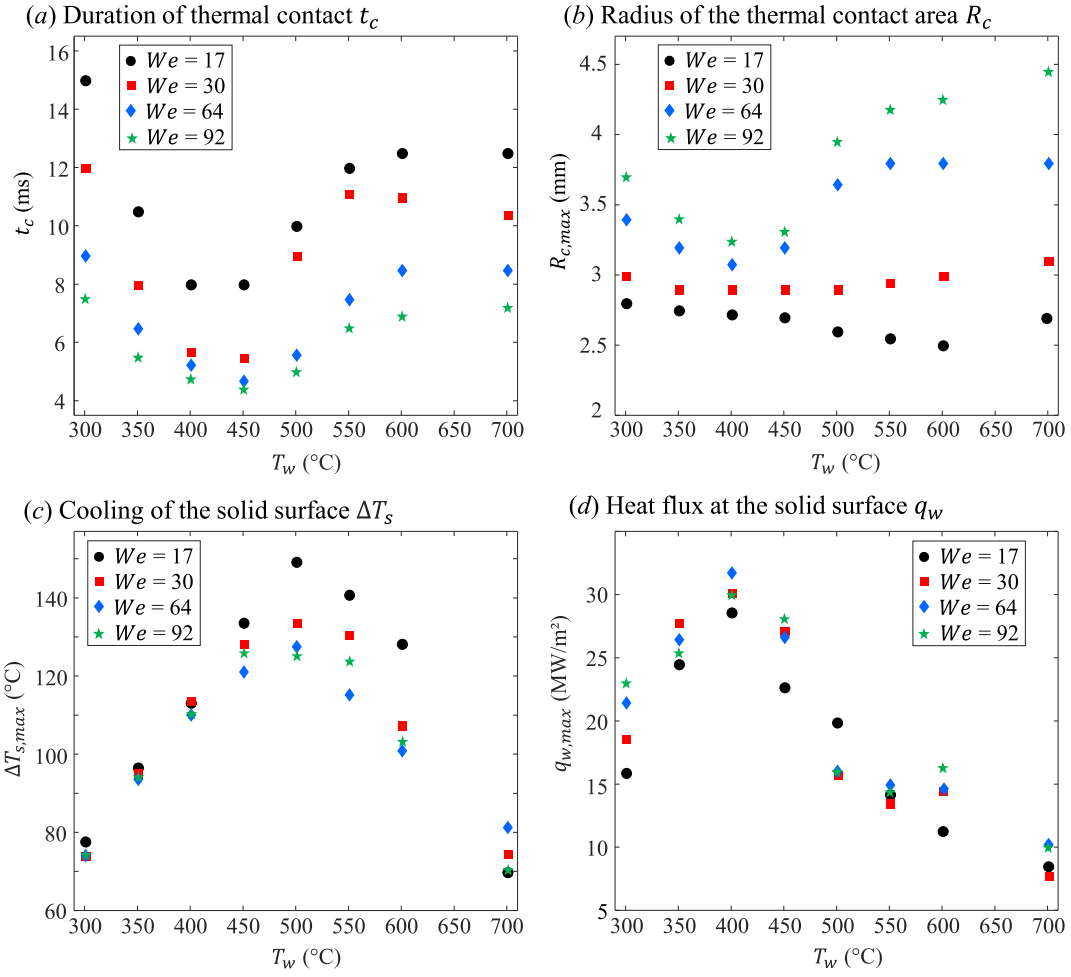

Fig. 19. Evolution of different parameters with the wall initial temperature T_{w0}: the duration of the thermal contact t_c (a), the radius of the thermal contact area (b), the cooling of the surface $\Delta T_{S,max} = T_{w0} - T_{S,min}$ (c), the maximum of heat flux q_w during the impact (d). In the inversion technique used to reconstruct the heat flux distribution, it was demonstrated by Chaze et al. [15] that a random noise on the temperature measurements only yields a noise in the estimated flux with no bias. Measurement uncertainties were therefore evaluated based on a repeatability study. This yielded an uncertainty of about 0.5 ms for t_c, 6% for $R_{c,max}$ and 10% for $q_{w,\,max}$. The measurement error for the surface temperature does not exceed 3°C at T_{w0}=300°C and 1°C at T_{w0}=600°C.

imaging. The error committed in the evaluation of Q_l is ignored, but it might be larger than Q_{vap}. In the film boiling regime, Q_l and Q_w are almost equal. Secondary atomization being less important, this indicates clearly that Q_{vap} plays a negligible role in the cooling.

- A minimum of Q_w is found around T_{w0}=450°C which corresponds to the LFP. However, it is not an absolute minimum, but simply a local minimum, which is weakly pronounced for the low *We* such as *We*=17 and *We*=30.
- It is possible to evaluate the cooling efficiency ε defined by:

$$\varepsilon = \frac{Q_w}{m_0\, Cp_l (T_{Sat} - T_{d0}) + L_v\, m_0}, \tag{24}$$

where m_0 is the initial mass of the droplet, and L_v=2260 kJ/kg is the latent heat of vaporization of water. Remembering the initial drop diameter d_0=2.6 mm, Eq. (24) leads to cooling efficiencies ranging from 2% et 6% in the film boiling regime, which is well in line with previous experimental studies such as Dunand et al. [30].

The variations of Q_w and Q_l displayed in Fig. 18 are the result of the combined effects of several parameters: the local heat flux, the contact time and contact area, which evolve in a complex manner with T_{w0}. To further describe the evolution of the heat transfer in the Leidenfrost transition, we introduce t_c as the thermal contact time (period during which heat transfer takes place) and R_c as the radius of the thermal contact area. By definition, $q_w(r, t)$=0 for $t > t_c$ and $r > R_c(t)$, so it can be written that:

$$Q_w \approx 2\pi \int_{t=0}^{t_c} \int_{r=0}^{R_c} q_w(r,t)\, r\, dr\, dt. \tag{25}$$

The values of t_c and R_c can be estimated from the distributions of q_w solving the inverse heat conduction model. Regarding the contact time t_c, this parameter can be evaluated with a rather good accuracy. However, a criterion had to be introduced for evaluating R_c due to the rather soft edge of the spatial distribution of q_w. The parameter R_c is determined so that Q_w calculated with Eq. (25) is 97% of the value given by Eq. (22). Fig. 19 (a) and (b) present the evolution of t_c and R_c as a function of the wall initial temperature T_{w0}. Since R_c varies during the impact, it was chosen to display $R_{c,max}$ (the maximum of R_c) in Fig. 19(b). The contact time t_c decreases in the bubbly boiling regime to a minimum around the LFP. Then, t_c increases to almost reach a plateau after 550°C in the film boiling regime. The impact velocity U_0 has a significant influence on t_c. The larger is U_0, the shorter is t_c.

Regarding the contact radius, $R_{c,max}$ decreases between 300°C and 400°C. However, the decrease is more pronounced for the high

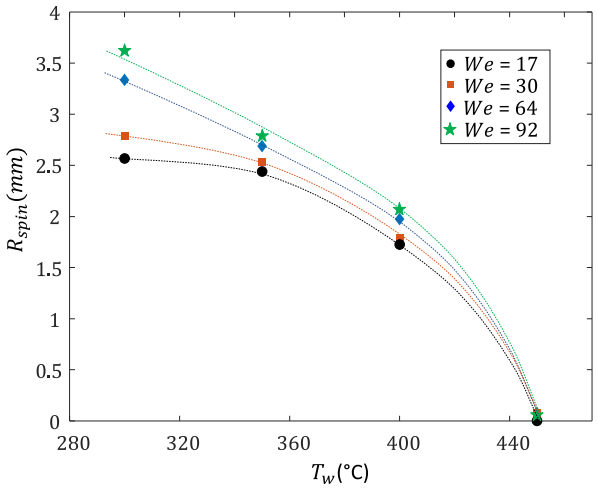

Fig. 20. Evolution of R_{spin} with the wall temperature T_{w0}. The smooth curves with dotted lines are introduced to highlight trends in these experimental data.

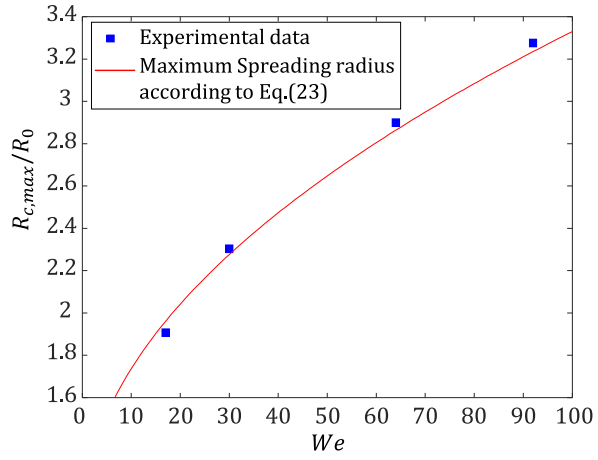

Fig. 21. Influence of We on the maximum radius of the thermal contact area $R_{c,max}$ in the film boiling regime (averaged values for $T_{w0} \geq 550$°C).

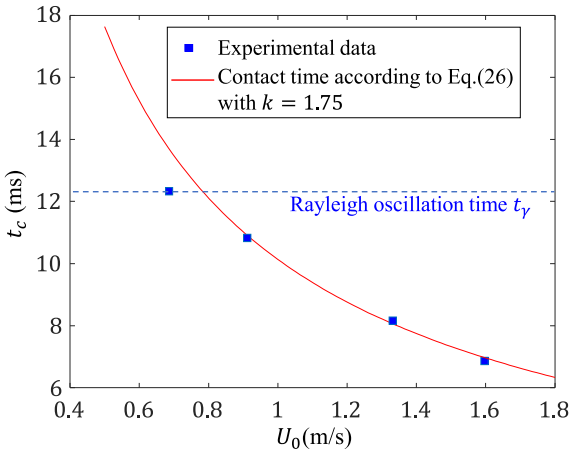

Fig. 22. Influence of the impact velocity U_0 on the thermal contact time t_c in the film boiling regime (averaged values for $T_{w0} \geq 550$°C).

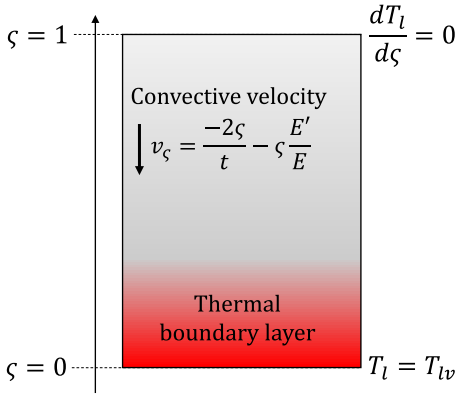

Fig. 23. Computational domain considered for the one-dimensional description of the heat transfer in the cylindrical slab of variable thickness $E(t)$ which features the spreading liquid lamella.

We. This yield to very close values of $R_{c,max}$ for the different We at 400°C. Increasing T_{w0} further in the film boiling regime, the values of $R_{c,max}$ deviate for the different We. $R_{c,max}$ increases with T_{w0} for We=64 and 92, but remains about constant for We=30 and decreases in the case of We=17. For $T_{w0} > 600$°C, $R_{c,max}$ tends to slightly increase for all the cases but variations are usually weaker.

Considering the variations of t_c and R_c for $T_{w0} > 550$°C, the decrease of Q_w in the same range of wall temperature, can only be explained by a reduction of q_w. In Fig. 19(d), the largest value of the wall heat flux q_w is observed at T_{w0}=400°C. In Fig. 19(c), the largest decrease in temperature of the solid surface $\Delta T_{S,max}$ is achieved between T_{w0}=450°C and 500°C. While it is sometimes alleged that q_w or the surface cooling $\Delta T_{S,max}$ reach a minimum at the LFP, this is clearly not the case for impacting droplets.

5.2. Heat transfer in the bubbly boiling regime

In the bubbly boiling regime, heat transfer is the most efficient in the wetting zone of the impact. At T_{w0}=300°C, our estimates of t_c and R_c are roughly the same as the wetting time and wetting radius obtained experimentally by Roisman et al. [21]. The latter also propose a model for the wetting contact time and radius accounting for the impact parameters. In this model, the lamella is assumed to detach from the solid surface when the thermal boundary layer, that develops from the lower surface of the droplet, reaches the top surface of the liquid lamella. Since the lamella is thinner on the edge, the wetting region is situated at the center while the periphery levitates. Knowing the residual thickness of the lamella h_{res} after the spreading, Roisman et al. [21] obtained an expression for the propagation of the wetting front solving h_{res}=h_t. This model compares well with their experimental results up to T_{w0}=300°C. But, when T_{w0} is higher than the spinodal temperature T_{spin}, this model fails as it predicts that the wetting time and the wetting radius do not evolve with T_{w0}. Introducing R_{spin} as the equivalent radius of the area defined by $T_S < T_{spin}$, Fig. 20 shows that R_{spin} tends towards 0 at the LFP. Given that R_{spin} is an upper limit for the wetting radius, the wetting area rapidly decreases and becomes less and less dependent on We when T_{w0} is approaching the LFP.

5.3. Heat transfer in the film boiling regime

Thermal contact radius As already described, fingers are approximately evenly distributed in space under the droplet. Their number is proportional to the radial distance r and does not depend on We (Fig. 15). Although there is locally important variations in heat flux in the space separating the fingers, globally the heat flux is distributed in a rather homogeneous way. The radius of thermal contact R_c is thus expected to compare with the spreading diameter. For water droplets in the film boiling regime, Castanet et al. [20] found experimentally that the maximum spreading di-

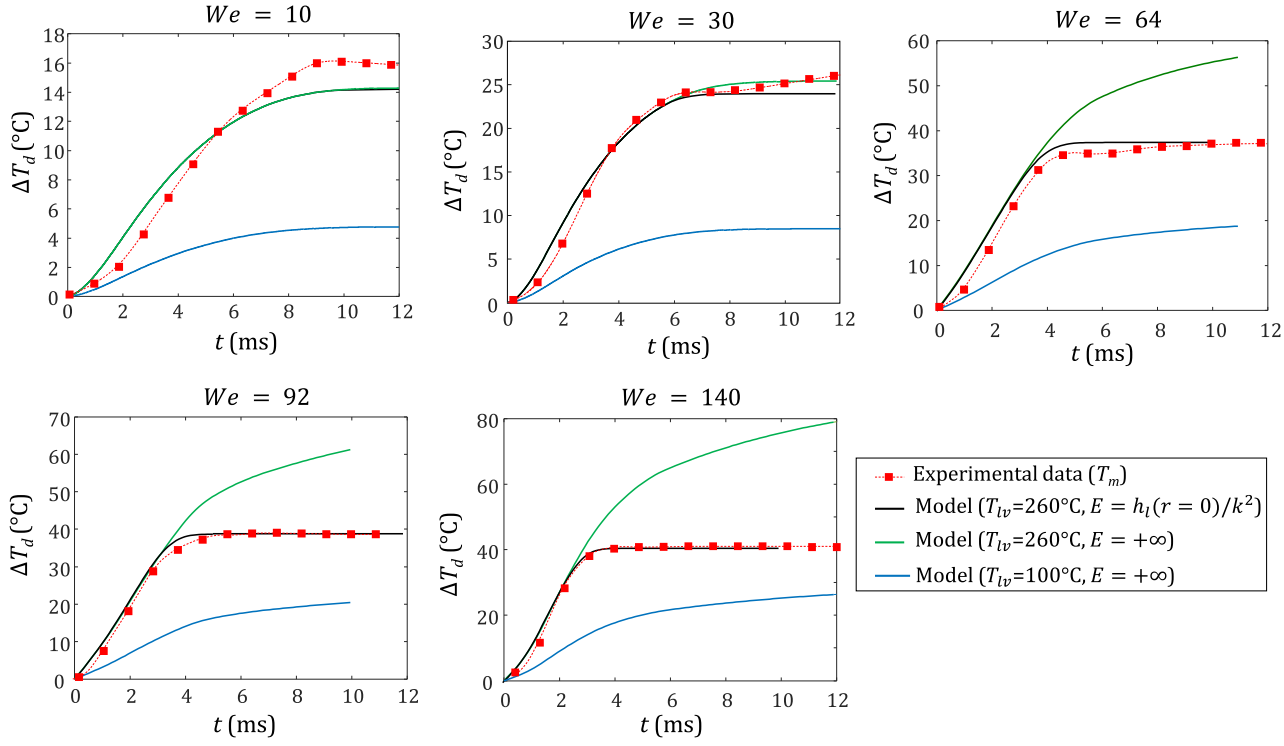

Fig. 24. Time evolution of the temperature of impinging water drops for different *We* at T_{w0}=600°C. Comparison between the theoretical model of drop heating and the measurements by 2cLIF thermometry.

ameter $d_{\max}$ can be well approximated by:

$$d_{max}/d_0 \approx 1 + 0.233\,We^{0.5}. \tag{26}$$

Fig. 21 shows that $R_{c,max}$ (the maximum radius of the thermal contact area during the impact) is effectively about equal to $d_{\max}/2$.

Duration of the thermal contact Except for *We*=17, the duration of thermal contact t_c is significantly shorter than the Rayleigh oscillation time $t_\gamma = \pi/4\sqrt{\rho d_0^3/\gamma}$, which is roughly equal to 12.3 ms presently. t_γ is a good approximation for the duration of the impact (time taken for the drop to spread, then retracts and leaves the wall surface). In fact, a thermal boundary layer develops within the droplet from its lower surface. Its thickness can be expressed by $h_t = k\sqrt{\alpha_l t}$, where k is a constant in the order of unity [16,25]. When h_t becomes approximately equal to the lamella thickness, the rate of heat transfer to the droplet drastically slows down, since heat cannot be dissipated efficiently from the top surface of the droplet. Provided sufficiently large *We*, the lamella thickness $h_l(r, t)$ can be determined by [28]:

$$\bar{h}_l = \frac{0.39}{\left(\bar{t}+0.25\right)^2}\exp\left[\frac{-2.34\bar{r}^2}{\left(\bar{t}+0.25\right)^2}\right],\quad \bar{h}_l \equiv \frac{h_l}{d_0},\quad \bar{r} \equiv \frac{r}{d_0},\quad \bar{t} \equiv \frac{tU_0}{d_0}. \tag{27}$$

Given the Gaussian shape of the lamella, the thermal contact lasts for a longer time at the center, meaning that:

$$h_l(r=0, t_c) = h_t(t_c). \tag{28}$$

For sufficiently large times, $h_l(r=0,t)$ can be replaced by $0.39/t^2$ and Eq. (28) yields:

$$t_c \approx \frac{0.686\,d_0^{6/5}}{k^{2/5}\alpha_l^{1/5}U_0^{4/5}}. \tag{29}$$

As shown in Fig. 22, Eq. (29) is in good agreement with the experiments for $k \approx 1.75$. However, if the impact velocity U_0 is low, this expression leads to a value of t_c that exceeds the Rayleigh oscillation time t_γ. In such case, the lamella thickness $h_l(r=0,\ t)$ remains higher than that of the thermal boundary layer h_t for the entire duration of the drop impact, and t_c is simply equal to t_γ. This situation presently occurs for *We*=17.

Modeling of the heat transfer Based on the above description, the heat transfer to the drop Q_l can be estimated within the frame of the same one-dimensional description presented in Section 4. The thermal problem is modified considering a liquid disk with a thickness $E(t)$ decreasing with time. To handle this problem with a free moving boundary, the vertical coordinate z can be substitued by $\varsigma = z/E(t)$. This allows to solve the heat equation in a domain with fixed boundaries as illustrated in Fig. 23. Using the above substitution, the heat equation (Eq. 5) can be rewritten as:

$$\frac{\partial T_l}{\partial t} - \left(\varsigma\frac{E'}{E} + \frac{2\varsigma}{t}\right)\cdot\frac{\partial T_l}{\partial \varsigma} = \frac{\alpha_l}{E^2}\cdot\frac{\partial^2 T_l}{\partial \varsigma^2}, \tag{30}$$

$$T_l = T_{lv} \text{ at } \varsigma = 0, \tag{31}$$

$$dT_l/d\varsigma = 0 \text{ at } \varsigma = 1. \tag{32}$$

The thickness of the liquid disk $E(t)$ shall be related to the thickness of the spreading lamella. To be consistent with the results presented in Fig. 22, $E(t)$ is defined as followed:

$$E(t) = \frac{h_l(r=0,t)}{k^2}. \tag{33}$$

The above problem is solved numerically using the finite element method. Once the temperature $T_l(\varsigma,\ t)$ has been calculated, the heat flux q_l entering the droplet is evaluated by:

$$q_l(t) = -\frac{\kappa_l}{E(t)}\left.\frac{\partial T_l}{\partial \varsigma}\right|_{\varsigma=0}. \tag{34}$$

Finally, the increase in the mean temperature of the drop $\Delta T_d = Q_l/mCp_l$ can be determined by:

$$\Delta T_d(t) = T_m(t) - T_{d0} = \frac{1}{m\,Cp_l}\int_0^t q_l(t)\cdot S_e(t)dt, \tag{35}$$

where $S_e(t)=\pi d_c(t)^2/4$ and d_c is the contact diameter. The time evolution of d_c can be determined using the theoretical approach developed by Castanet et al. [20], which is based on the application of momentum conservation to the rim bounding the liquid lamella. In the present study, $S_e(t)$ is evaluated from the drop contour on the images taken by laser-induced fluorescence.

The above heating model was compared to the measurements of the drop temperature obtained by 2cLIF at T_{w0}=600°C (Fig. 24). Experimental images of the drop temperature are averaged spatially to obtain the time evolution of the volume-average temperature T_m. To determine the temperature at the liquid/vapor interface T_{lv}, the results displayed in Fig. 17 should be used. In the case of T_{w0}=600°C, the contact temperature $T_{S,min}$ is about 495°C. Using Eq. (21), this corresponds to $T_{lv} \approx 260$°C. The theoretical model allows obtaining a good fitting of the experimental results for the different *We* (Fig. 24). In the same figure, the case of a semi-infinite droplet ($E \to +\infty$) and the case of non-superheated liquid interface (T_{lv}=T_{Sat}) are also presented. It is clear that taking into account the superheating of the liquid/vapor interface is critical in assessing the heat transfer to the drop.

Conclusion

The extremely rapid contact of a droplet which impinges on a superheated surface causes a very large superheating of the liquid. As long as the cooling of the surface occurring at the same time as the impact is sufficient, a wetting contact will take place. The dynamic LFP corresponds to the initial wall temperature for which the solid surface is cooled down to the temperature of the spinodal, i.e. the maximum temperature at which water can still exist in the liquid state. A model taking into account the heat transfer during the contact between the droplet and the wall, as well as the liquid flow in the spreading lamella, makes it possible to determine the dynamic LFP for sufficiently high Weber and Reynolds numbers. The Leidenfrost point is essentially a function of the thermal effusivity of the liquid and the wall. As the wall temperature approaches the LFP, the wetting area become narrows and the wetting lasts less and less time. Both parameters tending to 0, become less and less dependent on the Weber number. The LFP is neither a minimum of the heat flux nor a minimum of the surface cooling. When the wall temperature exceeds the LFP, the liquid at the vapor interface remains in a very high level of superheating and in the absence of a wetting contact, the homogeneous nucleation can play an important role. It induces the formation of a fingering pattern and to a certain extent leads to a secondary atomization of tiny droplets if the drop spreading is sufficiently large. The frictionless sliding of the liquid lamella onto the vapor cushion considerably help increasing the surface for the heat transfer, but this latter remains limited by the poor thermal conduction in the vapor film. For the high Weber numbers, the lamella becomes very thin during the spreading, which limits its ability to dissipate heat. This is due to the fact that the thickness of the thermal boundary layer is comparable to that of the lamella. This phenomenon can be considered in a one-dimensional description of the heat transfer. This model makes it possible to determine very precisely the quantity of heat evacuated by a drop in the film boiling regime. However, it is still necessary to know beforehand the liquid superheat at the liquid/vapor interface. A more comprehensive model is thus needed to predict this superheating. This model will certainly have to include the formation process of the fingers and the decrease of the liquid superheat induced by a more and more rapid growth of the vapor film when increasing the wall temperature.

Acknowledgments

The authors gratefully acknowledge the financial support of the CPER 2015–2020 ENERBATIN and of the European FEDER program.

References

[1] A.L. Yarin, I.V. Roisman, C. Tropea, Collision phenomena in liquids and solids, Cambridge University Press, 2017, doi:10.1017/9781316556580.

[2] A. Yarin, Drop impact dynamics: splashing, spreading, receding, bouncing, Annu. Rev. Fluid Mech. 38 (1) (2006) 159–192, doi: 10.1146/annurev.fluid.38. 050304.092144.

[3] J.D. Bernardin, C.J. Stebbins, I. Mudawar, Mapping of impact and heat transfer regimes of water drops impinging on a polished surface, Int. J. Heat Mass Transf. 40 (2) (1997) 247–267, doi:10.1016/0017-9310(96)00119-6.

[4] T. Tran, H.J.J. Staat, A. Prosperetti, C. Sun, D. Lohse, Drop impact on superheated surfaces, Phys. Rev. Lett. 108 (2012) 036101, doi:10.1103/PhysRevLett. 108.036101.

[5] V. Bertola, An impact regime map for water drops impacting on heated surfaces, Int. J. Heat Mass Transf. 85 (2015) 430–437, doi:10.1016/j.ijheatmasstransfer.2015.01.084.

[6] G. Liang, I. Mudawar, Review of drop impact on heated walls, Int. J. Heat Mass Transf. 106 (2017) 103–126.

[7] J.D. Bernardin, I. Mudawar, The leidenfrost point: experimental study and assessment of existing models, J. Heat Transfer. 121 (4) (1999) 894–903, doi:10.1115/1.2826080.

[8] C. Cai, I. Mudawar, H. Liu, C. Si, Theoretical leidenfrost point (lfp) model for sessile droplet, Int. J. Heat Mass Transf. 146 (2020) 118802, doi:10.1016/j.ijheatmasstransfer.2019.118802.

[9] W. Wagner, A. Pruss, The iapws formulation 1995 for the thermodynamic properties of ordinary water substance for general and scientific use, J. Phys. Chem. Ref. Data 31 (2) (2002) 387–535, doi: 10.1063/1.1461829.

[10] V. Carey, Liquid-Vapor phase-Change phenomena: An introduction to the ther- mophysics of vaporization and condensation in heat transfer equipment: An introduction to the thermophysics of vaporization & condensation in heat transfer equipment, Taylor & Francis, 1992.

[11] F.M. Tenzer, J. Hofmann, I.V. Roisman, C. Tropea, Leidenfrost temperature in sprays: role of the substrate and liquid properties, 2020.

[12] J.D. Bernardin, C.J. Stebbins, I. Mudawar, Effects of surface roughness on water droplet impact history and heat transfer regimes, Int. J. Heat Mass Transf. 40 (1) (1996) 73–88, doi:10.1016/S0017-9310(96)00067-1.

[13] L. Zhong, Z. Guo, Effect of surface topography and wettability on the leidenfrost effect, Nanoscale 9 (2017) 6219–6236, doi:10.1039/C7NR01845B.

[14] M. Khavari, C. Sun, D. Lohse, T. Tran, Fingering patterns during droplet impact on heated surfaces, Soft Matter 11 (2015) 3298–3303, doi:10.1039/c4sm02878c.

[15] W. Chaze, O. Caballina, G. Castanet, J.-F. Pierson, F. Lemoine, D. Maillet, Heat flux reconstruction by inversion of experimental infrared temperature mea- surements – application to the impact of a droplet in the film boiling regime, Int. J. Heat Mass Transf. 128 (2019) 469–478, doi: 10.1016/j.ijheatmasstransfer. 2018.08.069.

[16] G. Castanet, W. Chaze, O. Caballina, R. Collignon, F. Lemoine, Transient evolution of the heat transfer and the vapor film thickness at the drop impact in the regime of film boiling, Physics of Fluids 30 (12) (2018) 122109, doi: 10.1063/1.5059388.

[17] W. Chaze, O. Caballina, G. Castanet, F. Lemoine, Spatially and temporally resolved measurements of the temperature inside droplets impinging on a hot solid surface, Exp. Fluids 58 (8) (2017) 96, doi:10.1007/s00348-017-2375-1.

[18] D. Maillet, S. André, J.-C. Batsale, A. Degiovanni, C. Moyne, Thermal quadrupoles: Solving the heat equation through integral transforms, John Wi- ley & Sons Inc, 2000.

[19] W. Chaze, O. Caballina, G. Castanet, F. Lemoine, The saturation of the fluores- cence and its consequences for laser-induced fluorescence thermometry in liq- uid flows, Exp. Fluids 57 (4) (2016) 58, doi: 10.10 07/s0 0348- 016- 2142- 8.

[20] G. Castanet, O. Caballina, F. Lemoine, Drop spreading at the impact in the leidenfrost boiling, Physics of Fluids 27 (6) (2015) 063302, doi:10.1063/1.4922066.

[21] I.V. Roisman, J. Breitenbach, C. Tropea, Thermal atomisation of a liquid drop after impact onto a hot substrate, J. Fluid Mech. 842 (2018) 87–101, doi:10.1017/jfm.2018.123.

[22] M. Shirota, M.A.J. van Limbeek, C. Sun, A. Prosperetti, D. Lohse, Dynamic leidenfrost effect: relevant time and length scales, Phys. Rev. Lett. 116 (2016) 064501, doi:10.1103/PhysRevLett.116.064501.

[23] G.I. Taylor, The dynamics of thin sheets of fluid ii. waves on fluid sheets, Pro- ceedings of the Royal Society of London. Series A. Mathematical and Physical Sciences 253 (1274) (1959) 296–312, doi: 10.1098/rspa.1959.0195.

[24] G. Cossali, M. Marengo, M. Santini, Secondary atomisation produced by single drop vertical impacts onto heated surfaces, Exp. Therm. Fluid Sci. 29 (8) (2005) 937–946, doi: 10.1016/j.expthermflusci.20 04.12.0 03.

[25] J. Breitenbach, I.V. Roisman, C. Tropea, Heat transfer in the film boiling regime: single drop impact and spray cooling, Int. J. Heat Mass Transf. 110 (2017) 34–42, doi: 10.1016/j.ijheatmasstransfer.2017.03.004.

[26] A.L. Yarin, D.A. Weiss, Impact of drops on solid surfaces: self-similar capillary waves, and splashing as a new type of kinematic discontinuity, J. Fluid Mech. 283 (1995) 141–173, doi:10.1017/S0022112095002266.

[27] J.M. Kolinski, S.M. Rubinstein, S. Mandre, M.P. Brenner, D.A. Weitz, L. Mahade- van, Skating on a film of air: drops impacting on a surface, Phys. Rev. Lett. 108(2012) 074503, doi: 10.1103/PhysRevLett.108.074503.

[28] I.V. Roisman, E. Berberovi, C. Tropea, Inertia dominated drop collisions. i. on the universal flow in the lamella, Physics of Fluids 21 (5) (2009) 052103, doi: 10.1063/1.3129282.

[29] P. Van Carey, Liquid vapor phase change phenomena: An introduction to the thermophysics of vaporization and condensation processes in heat transfer equipment, second edition, 2018, doi:10.1201/9780203748756.

[30] P. Dunand, G. Castanet, M. Gradeck, D. Maillet, F. Lemoine, Energy balance of droplets impinging onto a wall heated above the leidenfrost temperature, Int. J. Heat Fluid Flow 44 (2013) 170–180, doi: 10.1016/j.ijheatfluidflow.2013.05.021.

[31] G. Agbaglah, C. Josserand, S. Zaleski, Longitudinal instability of a liquid rim, Physics of Fluids 25 (2013) 022103, doi:10.1063/1.4789971.